Tutorials in Optics

Duncan T. Moore, Editor

OSA Annual Meeting, Rochester NY

Optical Society of America • 2010 Massachusetts Avenue, NW • Washington, DC 20036

8

Methods for Characterizing Surface Topography

T. V. Vorburger
National Institute of Standards and Technology
Gaithersburg, Maryland 20899

Surface topography is important to the function of many kinds of industrial products, and the number of applications keeps increasing, making the need for adequate control of surfaces and an understanding of surface topography measurements more important than ever. This article presents a brief review of surface topography measurements. First, general ideas about surface topography, largely from ANSI/ASME Standard B-46.1,[1] are described. Next, stylus profiling techniques, in particular some of the parameters and statistics that result from measurements using these techniques, are described. Descriptions of optical and scanned probe methods for surface profiling follow and include some recent results. The article concludes with a short section on area techniques. For more extensive reviews of surface topography measurement, please see other sources.[2–4]

Figure 1 is similar to an illustration from the B-46.1 Standard on surface texture. It schematically shows a surface produced by a unidirectional machining process such as grinding. This surface has two orders of structure produced by different processes: the roughness and the waviness, each with a typical height and spacing. In general, roughness consists of closely spaced irregularities that may be produced by cutting-tool marks or by the grit of a grinding wheel, and waviness consists of widely spaced irregularities, often produced by vibration or chatter during the surface forming process. For many kinds of finishing processes these concepts are distinct, but for some machining processes it is difficult to distinguish between the two orders of structure. In addition to roughness and waviness, the standard also defines errors of form as long-period or noncyclic deviations from the ideal surface. These might be caused by errors in ways or spindles or by tool wear during machining. Finally, we distinguish flaws, which are discrete infrequent irregularities in the surface topography such as cracks, pits, and scratches. These are often caused by defects in the material itself.

It is conventional to define surface texture as comprising roughness and waviness only and to define surface topography as including errors of form and flaws as well as surface texture. However, many people tend to use the terms topography, roughness, and texture interchangeably. This paper primarily stresses the measurement of roughness.

1. Applications

The applications of roughness and texture measurements include traditional areas, such as automotive and other metal-working industries, in which roughness heights of the order of fractions of a micrometer are important to the function of sliding components.

The surfaces of hulls and propellers of ships should be smooth to the order of several micrometers to minimize hydrodynamic drag. However, the surface deterioration caused by the marine environment can produce peak–valley roughnesses of the order of several hundred micrometers.[5] Therefore, the maintenance of smooth surfaces is an important problem for the shipping industry.

Wind-tunnel models also require roughness and texture measurements. Our group in the Precision Engineering Division of the National Institute of Standards and Technology (NIST) has performed roughness measurements for the National Transonic Facility at NASA's

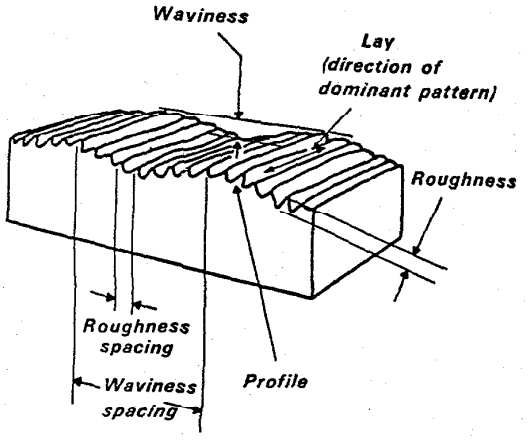

Fig. 1. Surface characteristics and terminology

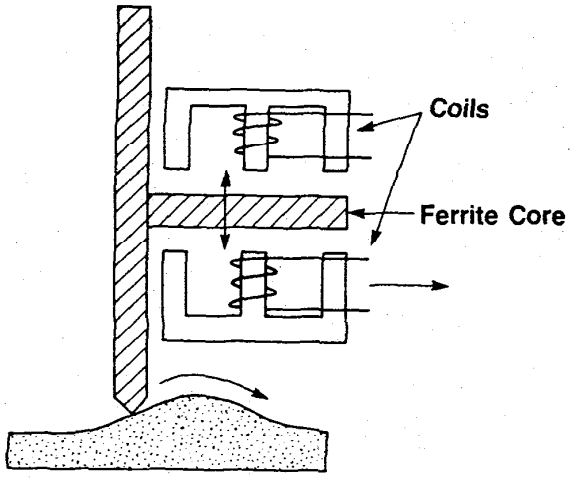

Fig. 2. Schematic diagram of LVDT stylus.

Langley Research Center. The aerodynamic models tested in that wind tunnel should have surface roughness heights less than 0.2 μm so that they are aerodynamically smooth under extreme conditions of flow.[6]

For optical and x-ray components, the smoother the surface the better, and roughness heights of 1 nm or less are necessary and are achieved.

Finally, the rates of certain surface chemical reactions may depend on the presence of steps on surfaces. Therefore, step heights and step densities may be cast as roughness parameters in the field of surface chemistry.

2. Surface Topographic Techniques

The field of roughness measurements may be divided into two kinds of techniques: profiling and area averaging. Profiling techniques measure surface heights point-by-point with a high-resolution probe such as a stylus or a focused optical beam. These techniques are usually accurate and quantitative. Measured surface profiles may be used to generate many statistical parameters and functions of the surface that characterize the average peak height or peak spacing.

We also include here bidirectional scanning methods such as the scanning tunneling microscope (STM), which yield three dimensional maps of surface topography, usually by accumulating and juxtaposing individual profiles in a raster fashion. The 3-D maps give a more complete visualization of the surface topography than individual profiles do, and are particularly valuable for distinguishing localized peaks and valleys from elongated features such as tool marks and grain boundaries. The maps also provide the data for a complete statistical description of a surface that characterizes its anisotropy.

By contrast, with area techniques a few measurements can yield a quantity that depends on some statistical average of the surface roughness. Because they rely on a few measurements or perhaps a single measurement, area techniques can be very fast and are thus potentially useful in automated manufacturing. However, because the results represent statistical averages of surface roughness properties, area techniques require physical models to derive geometrical parameters of the surface, such as the rms roughness,[1] from the measured parameters. Examples of area techniques include optical scatter, parallel-plate capacitance, and low-energy electron diffraction. Low-energy electron diffraction is ordinarily used by surface scientists for determining crystal structure, but it has also been used for estimating the average heights of steps and widths of ledges on surfaces at the atomic level.[7] In the following sections, we discuss a few of the more widely used methods for characterizing surface topography. Many other techniques have been developed and have important applications and are discussed elsewhere.[2–4]

2.1 Stylus Techniques

The discussion of profiling techniques will begin with stylus measurements. Figure 2 shows a stylus traveling over a surface bump. The sensor is a linear variable-differential transformer (LVDT).[8] As the stylus moves vertically, it changes the relative impedance of the coils and hence unbalances an ac bridge. The resulting signal is demodulated and amplified and yields a voltage proportional to the surface height. The lateral resolution of the instrument depends on the width of the stylus tip itself.[9] This is an important specification and it can be as small as 0.1 μm for the best types of styli.[10]

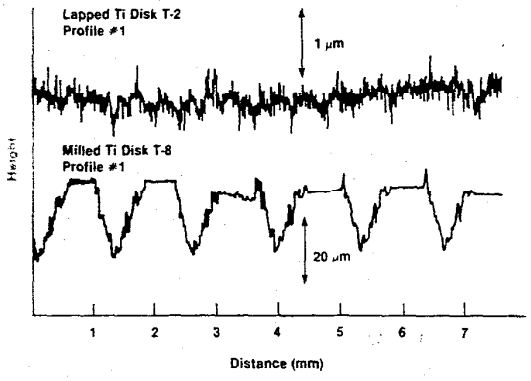

Fig. 3. Typical profiles measured with a stylus instrument.

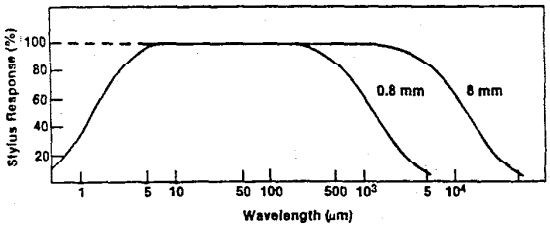

Fig. 4. Typical bandwidth limits for stylus instruments (from Ref. 1). The cutoffs for two RC filters are shown.

Figure 3 shows some typical height-versus-distance profiles obtained from a stylus instrument. These two profiles were measured for the Naval Ship Research and Development Center (NSRDC), which was investigating hydrodynamic drag on surfaces.[11] The surface represented in the upper curve was lapped to a finish with roughness heights less than 1 μm. The other surface was artificially roughened by ball end milling to produce increased drag, resulting in a highly periodic structure. The NSRDC group observed large differences in the hydrodynamic drags of these two and other components because of the differing degrees of roughness.

Figure 4, taken from ANSI Standard B-46.1,[1] shows typical lateral ranges of sensitivity for stylus profiling instruments. The sensitivity is unity in the middle of the range. It is limited at the short-wavelength end by the stylus tip width or often by the limitations in the high-frequency electronic response of the detection circuit. At the long-wavelength end the sensitivity may be limited by the actual length of the surface profile or by low-frequency resistance–capacitance (RC) filters that produce a long-wavelength cutoff. The use of RC filtering is standard practice in the mechanical parts industry[1] to distinguish roughness from waviness, but not in the optical industry.

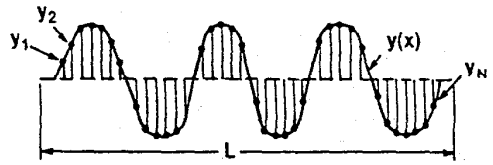

- R_a = Average Deviation of Profile y(x) from the mean Line
  = Total Shaded Area /L
  $= \frac{1}{L}\int_0^L |y(x)|dx \cong \frac{1}{N}\Sigma|y_i|$
- σ = rms Deviation...
  $\cong \sqrt{\frac{1}{N}\Sigma y_i^2}$
- R_{pv} = Peak to Valley Height
- Skewness (Q) $\cong \frac{1}{\sigma^3}\frac{1}{N}\Sigma y_i^3$

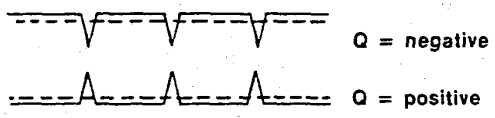

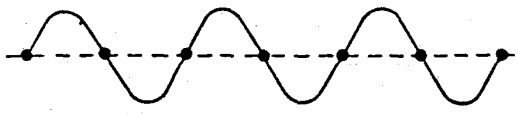

Wavelength:

- Peak-Count
- Average Wavelength
  $= 2\pi R_a$/Average Slope

Hybrid:

- Average slope

Fig. 5. Surface parameters.

Some useful surface parameters that may be calculated from a surface profile are shown in Fig. 5, which shows an idealized schematic profile $y(x)$ measured over a distance L. The profile may be digitized into N numbers, $y_1, y_2, \ldots, y_N$.

Perhaps the most widely used parameter outside the optical industry is the roughness average R_a, a height

parameter defined as the average deviation of the surface profile $y(x)$ from the mean line.[1] Geometrically it can be represented as the total ruled area divided by the evaluation length L. Analytically it is given by

$$R_a = \frac{1}{L}\int_0^L |y(x)|\,dx. \tag{1}$$

Digitally it is

$$R_a = \frac{1}{N}\sum_{i=1}^{N} |y_i|. \tag{2}$$

A second parameter, the rms roughness, often symbolized by σ in the optics community, is the rms deviation of the surface profile from the mean line. It is given by

$$\sigma = \left(\frac{1}{N}\sum_{i=1}^{N} y_i^2\right)^{1/2}, \tag{3}$$

and is a more conventional statistical quantity than R_a. Those two amplitude-averaging quantities are the most widely used for industrial specifications.

For some applications, the peak–valley height is an important parameter. It may be simply defined as the vertical distance R_{pv} from the highest peak on the profile to the lowest valley over the entire evaluation length of the profile. Several other peak–valley height parameters have also been defined to quantify the importance of the extreme peaks and valleys on surfaces to various functions of those surfaces.

The skewness Q is a shape parameter and is proportional to the third moment of the height distribution of the surface profile about the mean line (see Fig. 5). A similar parameter, called the kurtosis, is proportional to the fourth moment of the height distribution. Note that the first moment is equal to zero and the second moment is equal to the square of the rms roughness σ. Figure 5 illustrates a classic example of the importance of skewness for quantifying load-bearing capacities of surfaces. The two schematic profiles have the same R_a, the same peak–valley height, and the same spacings, but the skewness of one is negative and that of the other is positive, and the surfaces have very different load-bearing capabilities. The surface with negative skewness can bear loads much better than that with positive skewness.

The peak count and average wavelength are parameters that quantify surface spatial wavelengths. The peak count may be defined as the number of times the surface profile crosses the mean line in the positive-going direction over a specified length. The average wavelength (Fig. 5), developed by engineers in England,[12] is defined as 2π times the roughness average divided by the average slope Δ_a. If the surface were perfectly sinusoidal, this quantity would be exactly equal to the actual spatial wavelength of the surface. The average slope Δ_a itself is a hybrid parameter because it combines both height and distance information. It is ordinarily calculated by digital formulae[13] such as

$$\Delta_a = \sum_{i=1}^{N-1} \frac{|y_{i+1} - y_i|}{x_o}, \tag{4}$$

where x_0 is the lateral spacing of the digitized profile data.

Instead of trying to describe the profile in terms of a single parameter, it can be described better by a set of numbers, i.e., a statistical function. Two examples of the several functions that are used are the power spectral density and the probability density function. Figure 6 shows the power spectral density measured for two surfaces. The power spectral density is the square of the Fourier transform of the surface profile[2] and thus provides the decomposition of the surface profile into its wavelength components. The power spectral density is plotted

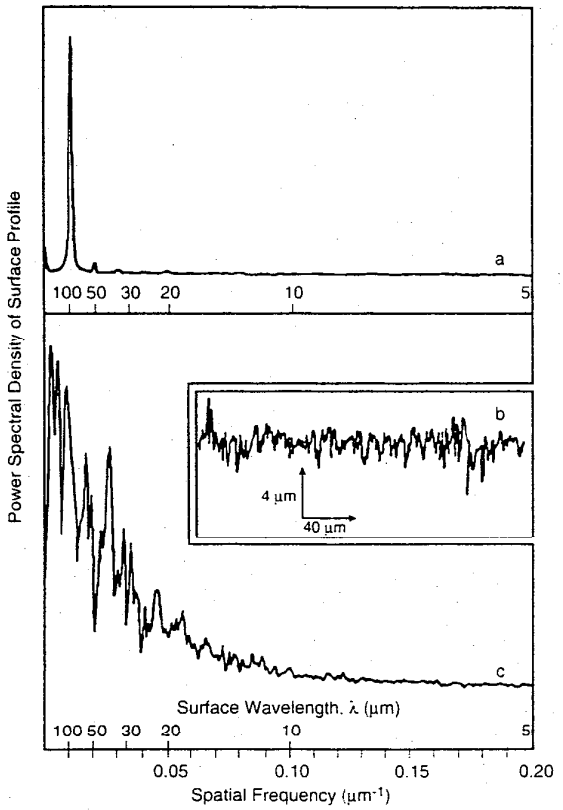

Fig. 6. Power spectral density functions for a sinusoidal roughness specimen (a) and a ground surface (c). A profile of the ground surface is also shown (b). The square root of the power spectral density is plotted here as the ordinate.

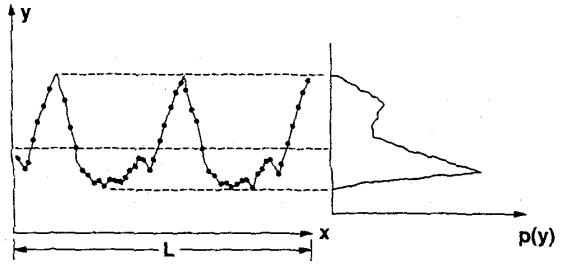

Fig. 7. Height density function (adapted from Ref. 14).

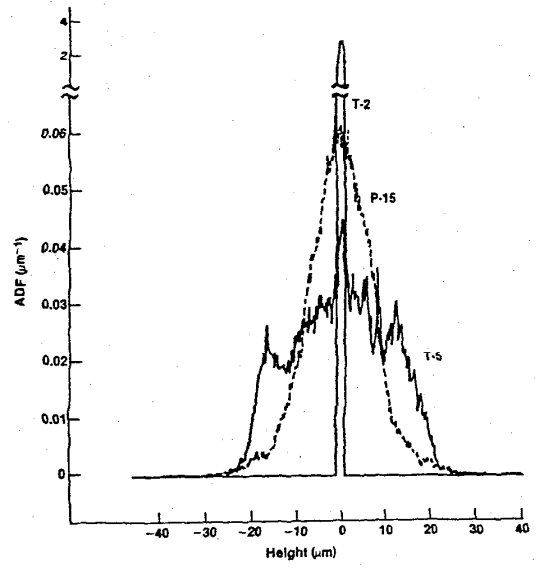

Fig. 8. Height density functions for three surfaces.

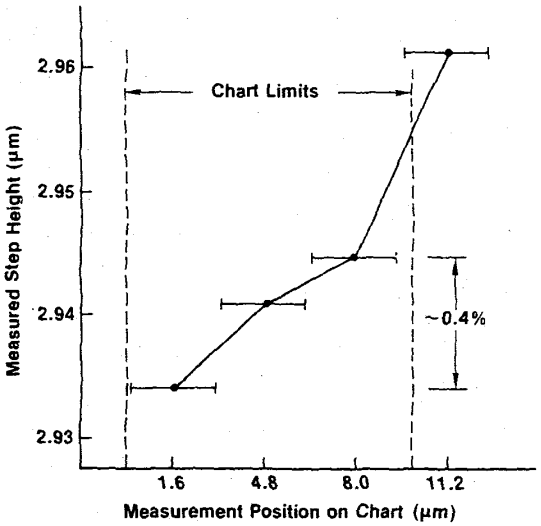

Fig. 9. Linearity test of LVDT stylus instrument.

as a function of the spatial frequency, the reciprocal of the surface spatial wavelength. The upper curve is for a nearly sinusoidal surface, which we use at NIST as a standard reference material. If it were a perfect sine wave, it would produce a single spike at the spatial wavelength of 100 μm with a width characteristic of the measured surface-profile length. This sinusoidal surface is not quite perfect, as is shown by the small harmonics in Fig. 6. In this case, the power spectral density is a good way to quantify the sinusoidal perfection of a surface. In contrast, the power spectrum of a ground surface replica is shown in the lower curve. The inset (b) is a profile of the replica. The ground surface replica is used as a comparison specimen for checking grinding operations. The power spectral density from the profile contains a lot of noise because of the finite sampling, but it is generally monotonically decreasing. As the surface wavelength gets shorter, the amplitude of the power spectral density decreases. This monotonically decreasing behavior is a typical result for most surface finishing operations. In addition, the function generally peaks and drops precipitously near dc ($\lambda = \infty$) either because of the low-frequency cutoff filters in the measuring instrument or because the dc level of the surface profile is subtracted before calculation of the power spectral density.

Another important function is the height density function, or amplitude density function.[14] This function is simply a histogram of surface heights. Figure 7 shows an example of a surface profile and the associated height density function. When the profile y is digitized and sorted into height bins, the height density curve $p(y)$ shown at the right is obtained. From both the profile and the height density function, it is clear that the surface profile is concentrated in the valleys. There is no spatial wavelength information here, but much height information is contained. Many of the height parameters of the surface, such as σ and Q, can be determined once the height density function[14] has been calculated.

Figure 8 shows three height density functions of components that we measured for the U.S. Navy. The periodic surface T-5 was produced by ball end milling. It has peaks at the high and low ends of the surface profile, as shown. Contrast that with the painted surface (P-15), which has considerable granularity, producing a random surface profile and yielding the nearly Gaussian height density function shown. The height density for the smooth, lapped surface, T-2, is a narrow spike when plotted on the same scale as the other two.

Finally, the accuracy and calibration of stylus instruments are important. Good accuracy requires a highly linear transducer. That is, measurement of the same surface height should not change over the range of the transducer. Figure 9 shows the results of a linearity test on a LVDT stylus instrument. It shows the variation in the results when a step height specimen is measured at four different places in the range of the LVDT. The 10-μm

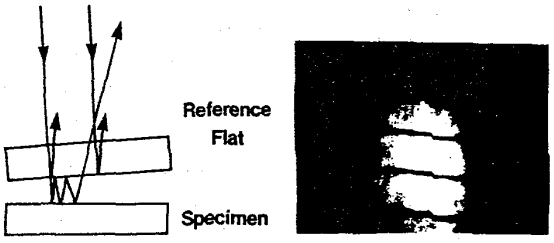

Fig. 10. Schematic diagram of a multiple-beam interferometer and interferogram of a 26-nm step.

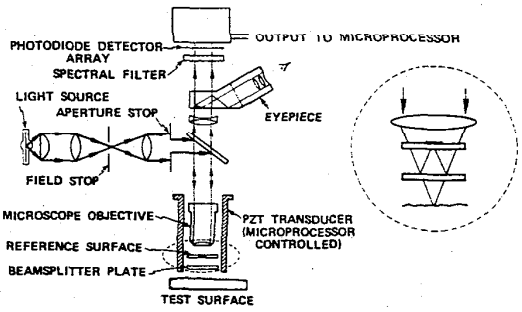

Fig. 11. Schematic diagram of a profiling interferometric microscope.

vertical range specified by the manufacturer is shown horizontally as the chart limits at the lowest magnification setting of the instrument. The four horizontal bars show the position and approximate height of a 2.94-μm step measured for each of four positions: low, medium, and high on the chart, and almost completely off scale. The measured values for the step height are plotted vertically. They were obtained by applying straight-line fitting routines to the low and high sides to give the step height. Ideally, the four bars should line up horizontally across the graph. The variation in the measured height over the chart width is fairly small—only about 0.4%—so the linearity is quite good. The linearity degrades slightly if one goes off scale, jumping by approximately 1%. This variation is typical of the linearity of many stylus instruments.

To calibrate the instruments, we use either calibrated step heights or periodic surfaces. The latter are easier to use and provide calibration of the instrument under the dynamic conditions of roughness measurement. However, step heights are usually more precise. Standard reference materials are available from NIST to calibrate profiling instruments.[15] These are sinusoidal roughness blocks with certified values of both R_a and spatial wavelength.

2.2 Optical Techniques

Optical profiling is a second way to acquire information regarding surface topography. Optical profilers are noncontacting and avoid the potential for surface damage associated with the contacting stylus. The optical instruments reviewed here are all interferometric, although there is another class of optical profilers, which are based on the detectability of the focus of a light beam on the surface[16] and have a vertical resolution nearly as good as that of the interferometers. Interferometric profilers have subnanometer vertical resolution, whereas focus-detection profilers have ~1 nm vertical resolution. Four types of optical interferometric profilers will be described: the profiling microscope, the scanning reference profiler, the circular path profiler, and the differential profiler.

By way of introduction, Fig. 10 shows a schematic diagram of a Tolansky[17] multiple-beam interferometer. The reference flat and specimen are located at the focus position of an optical microscope. The incident light is reflected from both the specimen and the bottom surface of the reference flat, which is in close proximity to the specimen but slightly displaced. The interference between the reflected beams produces fringes that represent surface profiles, as shown on the right. The special feature of this interferometer is the multiple reflection between the two surfaces, which sharpens the interference fringes. Hence, the multiple reflection improves the vertical resolution of the profiles. The NIST Precision Engineering Division has used this technique as one of several to measure the step heights used for calibration standards. The photograph on the right-hand side of Fig. 10 shows a 26-nm step, which was calibrated directly in terms of a half wavelength of the monochromatic sodium light source used here. One half-wave is represented by the spacings of the fringes. Multiple-beam interferometry has been useful for instrument calibration, but it requires manual analysis of the fringes or image analysis of the interferogram. Modern interferometers attempt to replace the manual analysis by automating the process with electronic phase measurements that also extend the resolution limit. The resolution of electronic phase-measuring interferometers is of the order of 0.1 nm or better.

Figure 11 shows a schematic diagram of a profiling interferometric microscope developed by Wyant *et al.*[18,19] In this version a Mirau interferometer is used. A slightly different design using a Fizeau interferometer has been developed by Smythe *et al.*[20] Light that passes through the objective of the microscope is separated into reference and test beams at the beam splitter. The interference between the light reflected from the reference surface and the test surface produces fringes sensed by the detector array. Surface height is quantified by using the piezoelectric transducer (PZT) to ramp the height of the reference surface and vary the phase of the interference fringes. Appropriate analysis of the sinusoidal intensity signal at

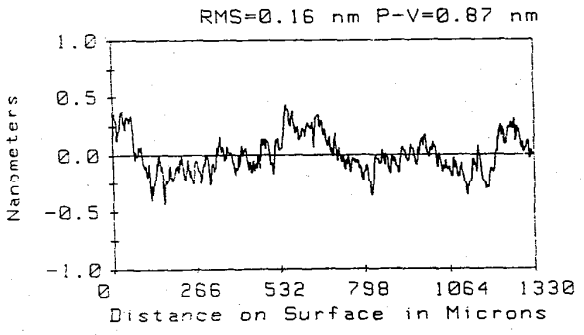

Fig. 12. Surface profile for a laser gyroscope mirror measured with an interferometric profiler (from Ref. 21).

each detector element yields its relative phase in the interference pattern and hence the relative height of each surface element. An interesting aspect of this interferometer and those described below is the way they handle the reference beam and the surface scanning. This instrument has no scanning motion at all. Its output is either a two-dimensional profile or a three-dimensional map obtained by electronic analysis of the linear or area detector array in the camera.

One limitation of the interferometric microscope is that profiling accuracy depends on the smoothness of the reference surface. On the other hand, because there is no scanning, there is no possibility of introducing profiling errors from extraneous motions of a scanning stage. Figure 12 shows a profile for a laser gyroscope mirror.[21] The indicated rms roughness is only 0.16 nm. Note that the trace length is approximately 1.33 mm. The finest wiggles on the profile illustrate the obtainable lateral resolution. For all the interferometers discussed here, the lateral resolution is in the range of 0.5–5 μm.

The interferometer shown schematically in Fig. 13 was developed by Downs *et al.*[22] It does not require a reference surface. A birefringent lens preceding the microscope objective splits the light into two polarization components. One component, the probe beam, is focused on the surface, and the other polarization component, the reference beam, is unfocused. The phase difference between these two components, the probe beam and the area-averaging reference beam, yields the surface profile. The principal limitation of this instrument is that the reference beam area is only approximately 10 μm in diameter. Therefore, although there is no need here for a nearly perfect reference surface, the range of measurable spatial wavelengths is limited by the 1–2-μm size of the probe beam and the approximate 10-μm width of the reference beam. Otherwise, the instrument gives highly precise surface profiles and has a vertical resolution better than 0.1.

A similar instrument, which also avoids the use of a reference surface and which I call the circular path profiler, is shown in Fig. 14. It is based on a design of Sommargren[23] and was developed by Smythe.[24,25] The incoming beam is divided into its two polarization components by the Wollaston prism, and these components are focused at different places on the sample. The reflected beams are then recombined at the Wollaston prism. The reference beam is coincident with the axis of rotation of the sample, and the measuring beam traces a circular path on the sample surface as the sample is rotated. The result-

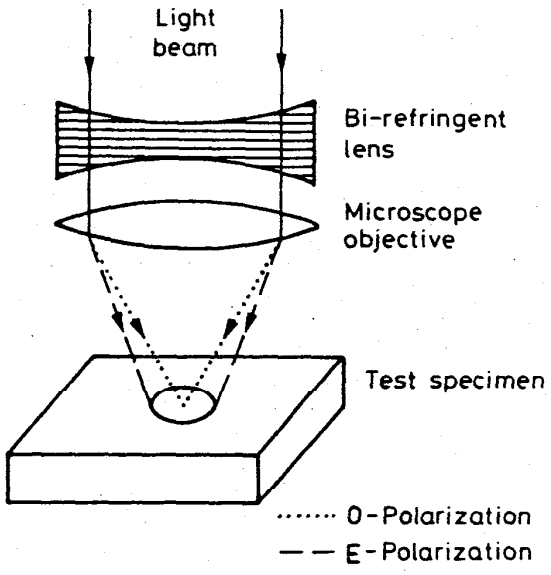

Fig. 13. Schematic diagram of the polarization profiler developed by Downs *et al.* (from Ref. 22).

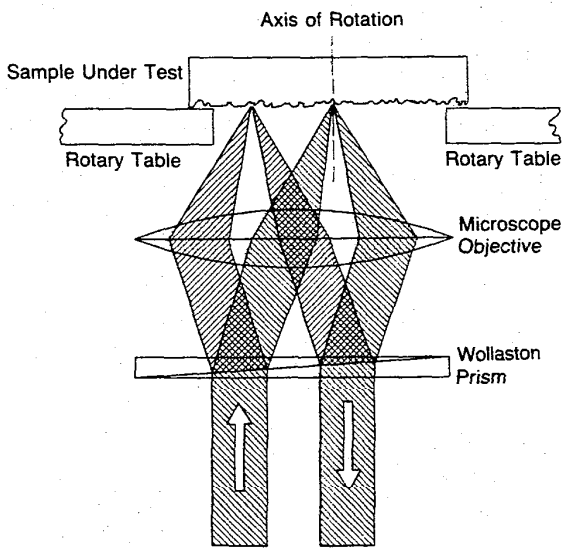

Fig. 14. Schematic detail of circular path profiler.

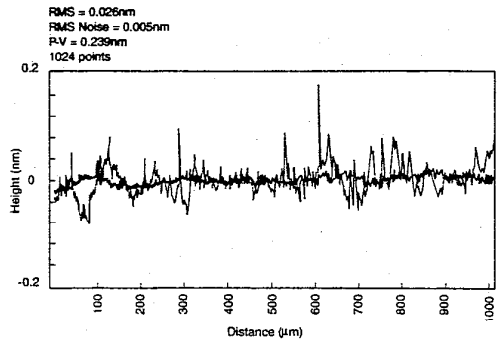

Fig. 15. Surface profile of fused silica substrate measured by a circular path profiler (gray). Noise profile (black).

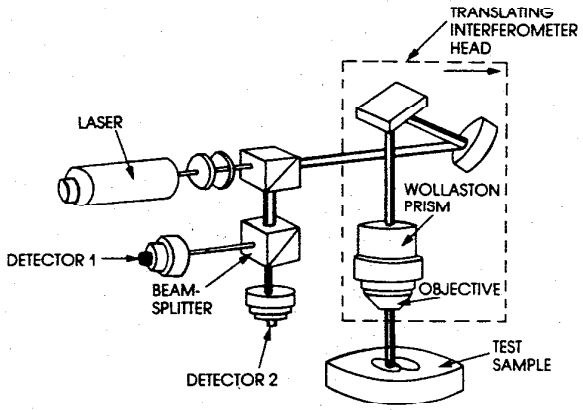

Fig. 16. Schematic diagram of differential profiler (from Ref. 27).

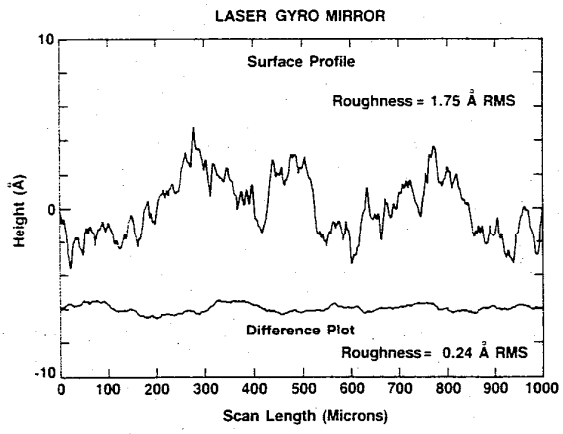

Fig. 17. Surface profile of laser gyroscope mirror measured with differential profiler (from Ref. 21).

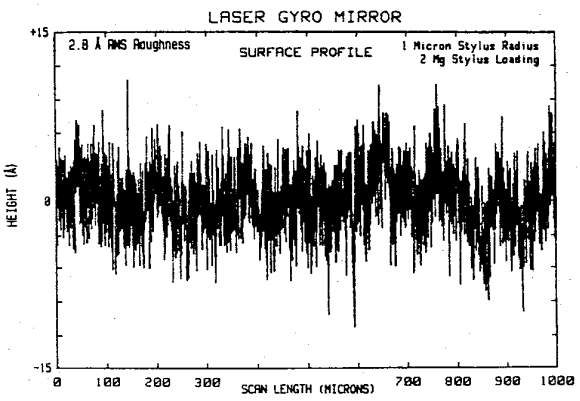

Fig. 18. Surface profile of laser gyroscope mirror obtained with a high resolution stylus instrument (from Ref. 21).

ing surface profiles are circular and are defined by the phase difference between the probe beam at the traversing point and the stationary reference beam. Because of the tight mechanical design, the vertical resolution is excellent. The principal limitation is the circular profile geometry with fixed length of ~1 mm.

Figure 15 demonstrates both the vertical resolution capability of the circular path profiler and the quality of the best optical surfaces.[24,25] It shows a surface profile of a fused-silica sample with a measured rms roughness of 0.026 nm. The noise curve was measured while the instrument was held stationary without rotating, and its effective rms roughness is approximately 0.005 nm.

A third instrument with two beam-probing is the differential profiler of Eastman[26] and Bristow *et al.*[27] (see Fig. 16). This instrument has a Wollaston prism design similar to that of the circular profiler, but instead of moving in a circular direction it scans linearly and produces profiles of the surface up to 100 mm in length. The profiles are produced by successive integration of the differential height measurements along the line of traverse. A key feature of this instrument is its ability to measure a long profile. There is potential for accumulating error in the profile from the integration procedure, but, in fact, over a length of 1 mm the profiles of smooth surfaces are comparable to those obtained for other instruments. Figure 17 shows the surface profile of a laser gyroscope mirror produced on this interferometer. The mirror has a measured roughness of 0.175 nm. Below the surface profile is another calculated from the difference between successive profile measurements. The difference plot has an effective rms roughness of 0.024 nm (0.24 Å) and illustrates the repeatability of the instrument. The profile of Fig. 17 is similar to the profiles obtained with the other optical profilers (Figs. 12 and 15). By contrast, the stylus profile of a laser gyroscope mirror (Fig. 18) shows much more

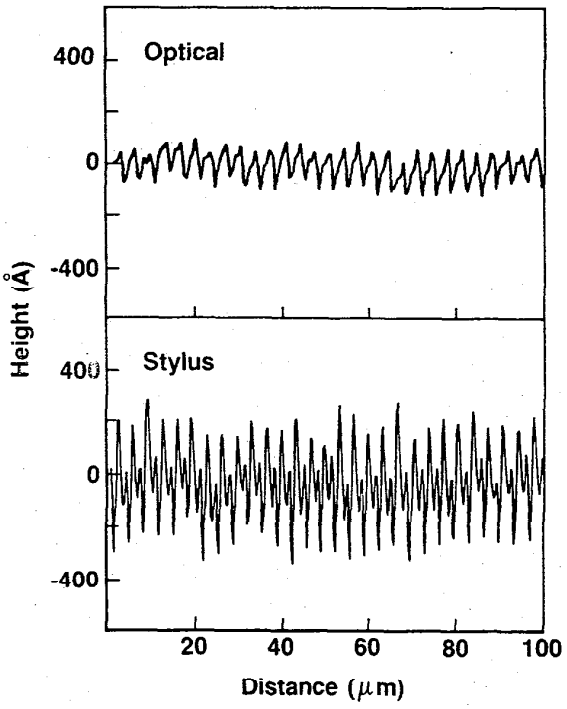

Fig. 19. Profiles of machined silicon (from Ref. 28).

closely spaced structures. This is not instrument noise. Stylus instruments can actually probe with a lateral resolution as small as 0.1 μm with a tip of that size and with a small stylus loading.[10]

Several years ago, Church *et al.*[28] compared spatial-frequency data from the interferometric profiler with those of the stylus. The sample was a periodic silicon surface machined by single-point flycutting, a process that produced a highly periodic surface with two sets of grooves of the same periodicity but different amplitudes. As shown in Fig. 19, this structure was not resolved by the interferometric profiler but was resolved by the stylus. The profile shape was not an artifact resulting from the mechanical dynamics of the stylus instrument because measurements made at different speeds produced the same profile. However, the power spectra (not shown) illustrated an interesting limitation of the stylus instrument: frequency modulation from the variation in velocity of the probe as it translated over the surface. Frequency modulation was not observed in the power spectrum from the interferometric profile because measurement of the displacement along the surface depended on the accuracy of separation of the elements in the linear array, which was very precise.

To improve the lateral resolution of optical profilers, Wyant *et al.* have developed a Linnik-type interferometer,[29] which operates at higher magnification than the Mirau design of Fig. 11. Figure 20 illustrates its capability

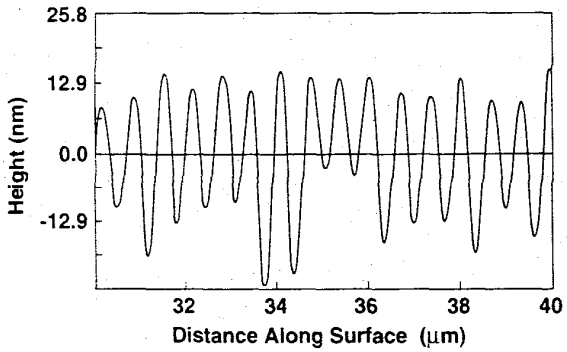

Fig. 20. Surface profile of holographic grating measured by interferometric profiler with high-resolution Linnik-type head. (J. C. Wyant, private communication.)

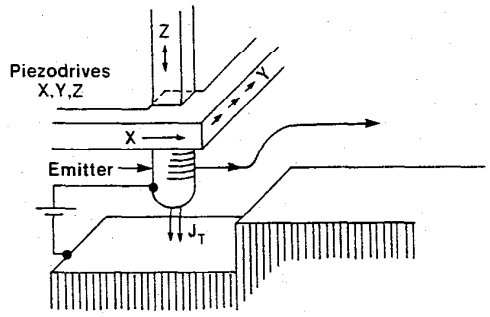

Fig. 21. Schematic diagram of STM.

for sensing high-frequency surface structure. The spacing of the holographic grating is only 0.67 μm.

2.3 Recent Scanned Probe Techniques

During the 1980s several new sensor concepts were successfully applied to high resolution surface profiling. The first to be developed was the scanning tunneling microscope (STM). Figure 21 shows a schematic diagram of a STM from the work of Binnig and Rohrer,[30] for which they won the Nobel Prize in physics. The early work on the principle of operation for this kind of instrument was done by Young *et al.*[31] at NIST. However, Binnig and Rohrer were the first to obtain atomic resolution with a tunneling microscope. A conducting tip is held very close (within 1 nm or less) to a conducting surface. A voltage is maintained between the tip and the surface. The resulting tunneling current of electrons passing through the gap is an exponential function of distance, thus providing a strong sensitivity to surface height when the tip is scanned

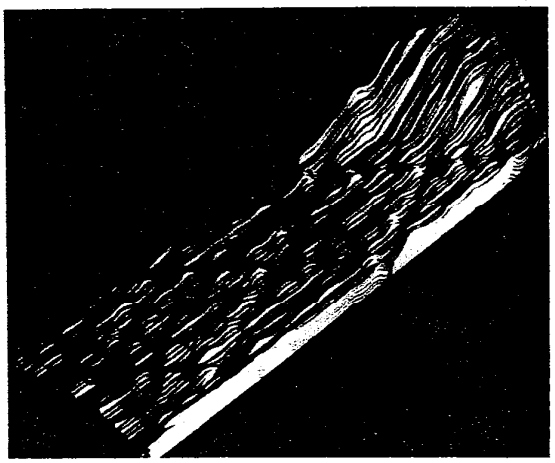

Fig. 22. STM image of Si(111) measured by Binnig *et al.* (from Ref. 32).

laterally. A piezoelectric transducer (Z) can vary the vertical distance between the tip and the surface. While scanning, a servo system maintains constant tunneling current by adjustment of the tip-to-surface distance. The resulting voltage signals to the piezodrive (Z) are proportional to the surface topographic heights over the scanned area, provided the tunneling current is not influenced by any variations in the surface material.

Figure 22 shows early dramatic evidence[32] of the resolution capabilities of the instrument. It is a set of profiles forming a map of a silicon (111) crystal surface that was annealed so that it produced a 7 × 7 low-energy electron diffraction pattern on the surface. Controversy existed over the true structure of this surface until Binnig *et al.* observed the structure directly, but the lateral resolution of the map, which shows the individual atomic peaks and holes, is more central to this review. The spacing between adjacent peaks here is approximately 0.8 nm. Much research and the development of many instruments for imaging conducting surfaces with atomic resolution followed Bennig *et al.*'s measurement.

The STM is useful for applications other than those in surface science. Figure 23 shows the result of a measurement of the surface of a grating by Dragoset *et al.*[33,34] of NIST. The grating had 2200 lines/mm, a 0.46-μm period. The STM shows imperfections in the structure of the grating between the lines. A high-resolution stylus instrument was able to resolve the grating lines but was not able to see the structure between the lines.

Figure 24 is a STM map of a gold surface machined by diamond turning with a feed spacing of 100 nm.[33] A stylus instrument was not able to resolve the individual

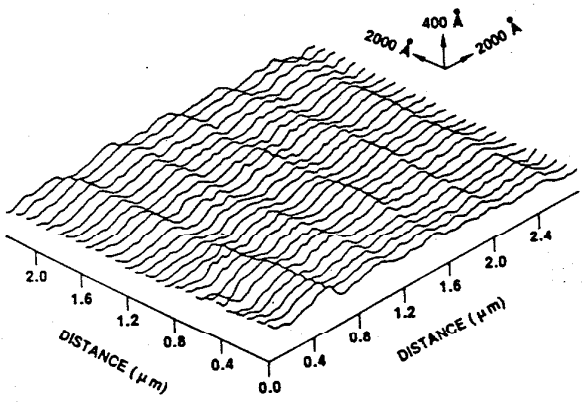

Fig. 23. STM of gold grating replica (from Ref. 33).

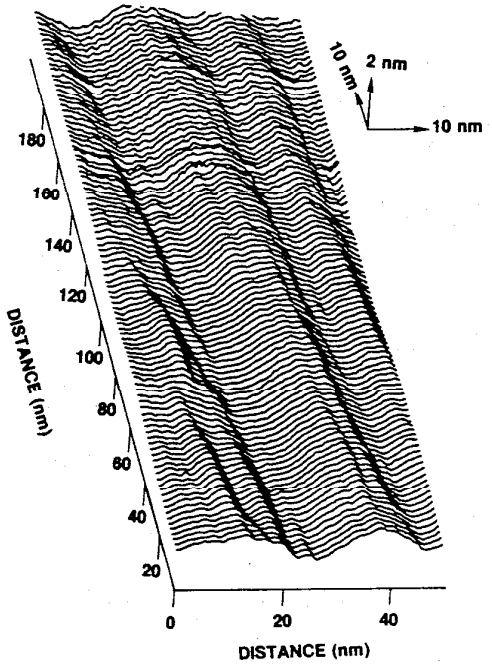

Fig. 24. STM of diamond-turned gold surface (from Ref. 33).

feed marks, but the STM was. In fact, this map shows the structural imperfections along the direction of travel of the tool over a width of 50 nm, half the period of the feed. Thus, this technique holds the promise of more sensitive measurements of optical surfaces, which could lead to better manufacturing techniques.

There have been several spinoffs of the STM that use other types of sensing mechanisms.[35–38] One of these is the atomic force microscope (AFM), first developed by Binnig *et al.*[38] There are several types of AFM sensors.

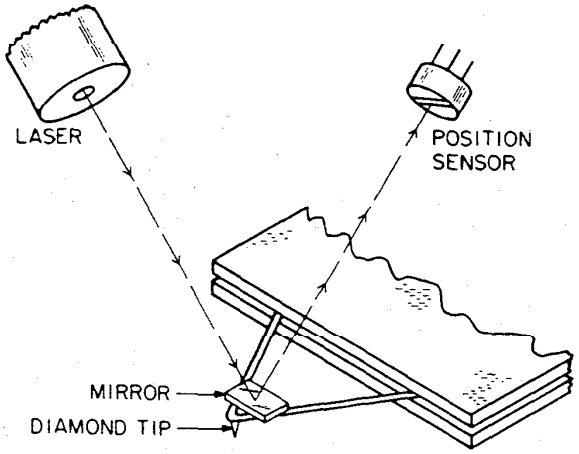

Fig. 25. Schematic diagram of AFM with optical lever sensor (from Ref. 39).

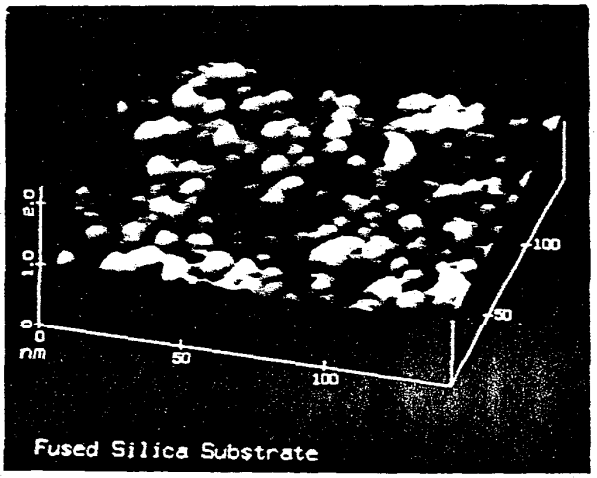

Fig. 27. AFM image of fused silica (from Ref. 41).

Fig. 26. AFM image of polished aluminum (from Ref. 40).

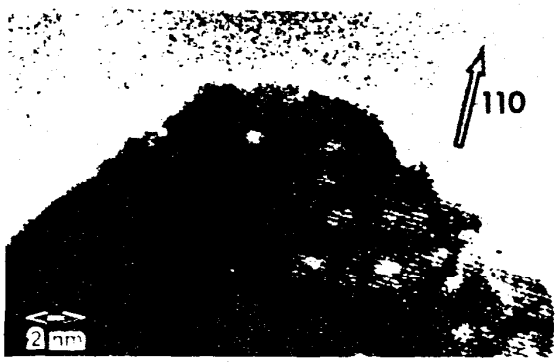

Fig. 28. Scanning electron microscope image of ion-milled tungsten tip used for STM (from Ref. 42).

Nearly all of them detect the deflection of a small cantilever probe as it contacts the surface. The forces of contact are controllable to the order of 10^{-8}–10^{-10} N, and the systems have been operated in both the attractive and repulsive modes. The first design by Binnig *et al.* used a STM to sense the cantilever deflections, but a more widely used approach nowadays is an optical lever sensor,[39] an example of which is shown in Fig. 25. A key advantage of the AFM is its ability to profile insulating as well as conducting surfaces, whereas the STM is limited to conductors. This gives the AFM great potential as a high-resolution profiler of optical surfaces. One example of the AFM capability is the map of polished aluminum from Elings *et al.*[40] shown in Fig. 26. Aluminum is very difficult to measure with a STM because in air it naturally forms a thick, insulating oxide. The field of view here is about 25 μm × 25 μm, illustrating that the AFM (and STM as well) is capable of scanning over macroscopic distances. However, lateral details as small as ~0.3 μm across are well resolved in this map. A map of fused silica taken by Bennett *et al.*[41] at higher resolution is shown as Fig. 27. The field of view is ~(150 nm)^2, and peaks of 5 nm across or less are clearly resolvable. With quantitative maps like these measured at such high resolution, it seems likely that a new era has begun in the quality control of optical surfaces based on high-resolution profiling.

Both the STM and AFM depend on the quality of the probe tip. In the early days of scanning tunneling microscopy, the high resolution was somewhat uncontrollable and most tips were produced by "cookbook" methods. By contrast, Fig. 28 illustrates an early example of a tungsten STM tip produced systematically.[42] The tip yielded

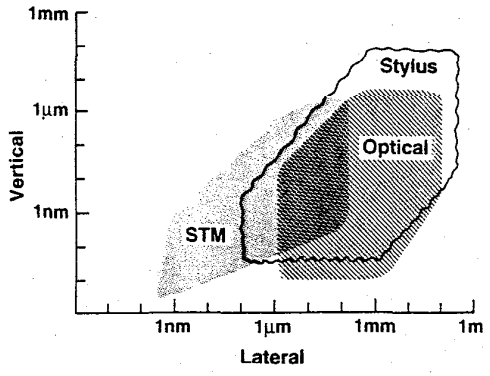

Fig. 29. Comparison of range and resolution of three profiling techniques.

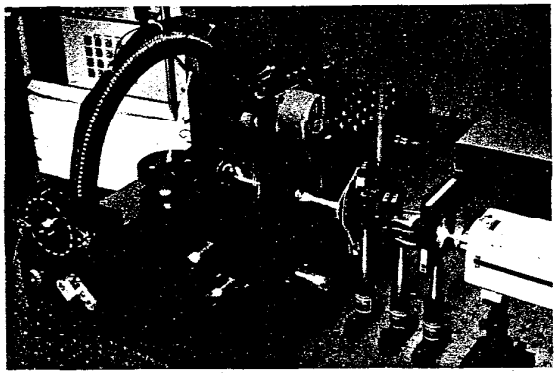

Fig. 30. Photograph of DALLAS–detector array for laser light angular scattering.

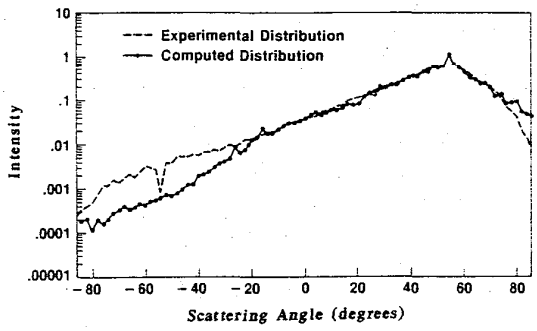

Fig. 31. Comparison of scattering experiment measured with DALLAS and theoretical results for hand-lapped stainless steel surface with rms roughness of 0.22 μm. The angle of incidence is −54°.

atomic resolution when used in a STM. It was produced by an ion-beam milling process in which the tip was rotated about an axis during milling in a manner similar to a turning operation. The milled probe tip is a single crystal and is approximately 8 nm across.

The range and resolution of three profiling techniques—STM, stylus, and optical interferometry—are summarized in Fig. 29. This graph is conceptually similar to others produced by Church[43] and Stedman.[44] It shows the resolution and range in both the lateral and vertical directions as the edges of the various areas. The vertical resolution is of the order of 0.05 nm for the most sensitive stylus instruments, whereas the vertical range can be of the order of 1 mm for stylus instruments used for the mechanical parts industry. The lateral resolution can be as small as 0.1 μm, depending on the quality of the stylus tip.[10] The vertical resolution of optical instruments is even better, but the lateral resolution is a modest 0.5–1 μm limited by the diffraction of visible light. The STM has both atomic lateral resolution and subatomic vertical resolution, and its lateral range is approximately 200 μm,[45] limited partly by the accuracy of long travel motion and partly by the ability of the servo system to respond to sudden large changes in the measured height signal, which are likely to occur when defects are encountered during rapid scans over long distances.

2.4 Area Techniques

This section emphasizes optical scattering. Parallel-plate capacitance[46,47] and low-energy electron diffraction[7] have also received practical application and are discussed elsewhere.

Two applications of optical scattering are discussed. The first application is directed toward the need in the mechanical parts industry for a reliable, high-speed measuring technique for use on rough surfaces produced in an automated manufacturing environment. Figure 30 shows an experimental apparatus[48] for measuring how these types of surfaces scatter light. A helium–neon laser beam illuminates the test surface, which is mounted at the center of a yoke holding 87 detectors spaced 2° apart. Each detector consists of a lens that focuses the scattered radiation into an optical fiber. The radiation is directed through the fiber to a PIN silicon photodiode. The bank of fibers and photodiodes is shown in the background. The output of the photodiodes is processed by a computer to produce angle-resolved scatter intensity distributions.

The samples in the initial experiments were produced by a unidirectional machining operation to keep the geometrical analysis simplified to two-dimensional problems. The results of one set of measurements[49] are shown in Fig. 31. Here the light is incident at an angle of −54°, so specular scattering is observed at +54°. The dashed curve shows the scattering intensity distribution gathered by the

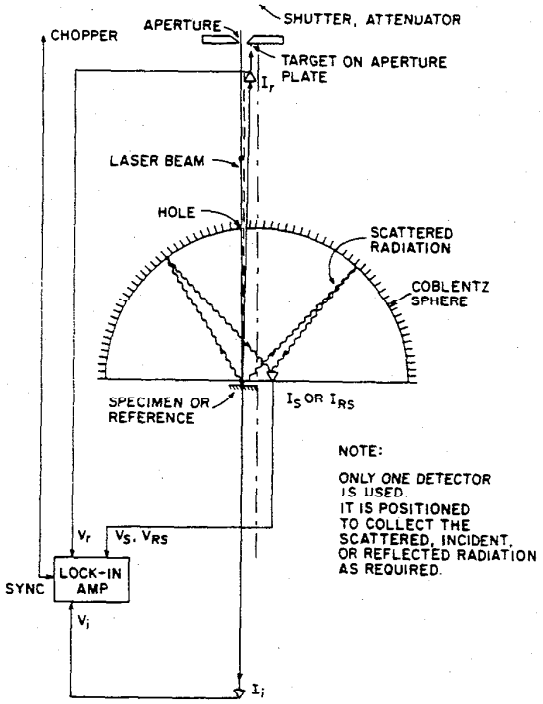

Fig. 32. Schematic diagram of a TIS apparatus (from Refs. 53 and 54).

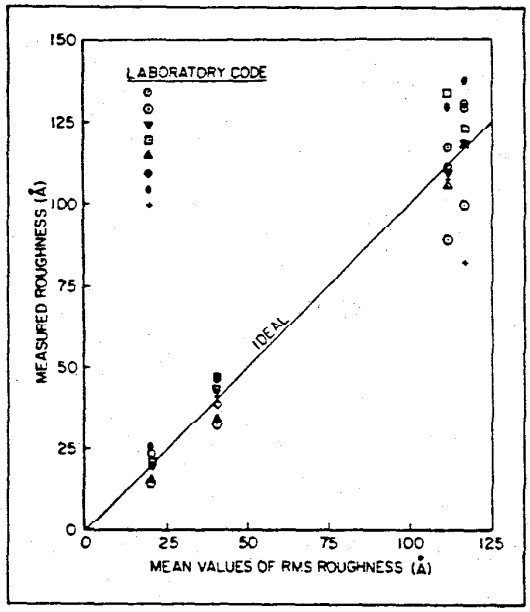

Fig. 33. Measured values of rms roughness obtained by TIS measurements at eight different laboratories (from Ref. 54).

detectors plotted over approximately four orders of magnitude. The valley at -54° is an artifact resulting from blocking of one of the detectors by the cantilevered mirror directing the incident optical beam.

The experimental curve is compared with a calculation based on detailed surface profiles measured with a stylus. The agreement between them is very good except for a region at high scattering angles (-80° to -30°). The disagreement there is probably from the 0.5 μm width of the stylus, which limits it in measuring closely spaced surface features. This graph demonstrates a fairly quantitative understanding of optical scattering from moderately rough surfaces. Other research has been directed toward the inverse problem,[50] i.e., using the scattering information to predict statistical parameters of the surface, such as rms roughness[50] or surface slopes.[51,52]

Figure 32 shows the schematic diagram for another application of optical scattering to surface roughness analysis known as total integrated scattering (TIS). The details of the measurement are specified in ASTM Standard F1048.[53] Light from a helium–neon laser is incident on the specimen from above. If the surface were perfectly smooth, the reflected light would be returned through the entrance hole, but if the surface has some roughness, light is scattered into the hemispherical collecting mirror (Coblentz sphere) and focused onto a detector (I_s). The scattered light intensity, for surfaces with roughnesses less than ~15 nm, is proportional to the square of the rms surface roughness.

Figure 33 shows a comparison of a round robin series of TIS measurements[54] made by several different laboratories for four surfaces. The agreement between them, although not perfect, was good enough to form a basis for the standard.

3. Concluding Observations

There have been dramatic advances in profiling instruments for measuring surface topography. Stylus instruments have shown improvements in resolution, and optical profiling instruments have improved dramatically over the past several years in their vertical resolution and capability for three-dimensional mapping. The STM and the AFM are revolutionary instruments that are now commercially available. Area techniques have also advanced for manufactured surfaces, particularly angle-resolved light scattering and total integrated scattering. A standard based on total integrated scattering now exists.

Several major technical challenges also exist. First, if the STM and AFM are to be generally useful for a wide class of industrial applications, probe tips must be accu-

rately measured and controlled. Second, techniques must be found to use the new measurement capabilities for improved control of optical and mechanical products. Otherwise, the resolution capabilities of these instruments are superfluous. Third, the requirements for the calibration of these instruments must be recognized. The situation with stylus instruments is satisfactory, but optical instruments and the STM require new efforts.

Acknowledgments

The contributions of a number of colleagues are gratefully acknowledged: J. M. Bennett, D. K. Biegelsen, T. C. Bristow, E. L. Church, J. A. Detrio, M. J. Downs, R. A. Dragoset, V. B. Elings, C. Giauque, D. Gilsinn, P. Hansma, F. Mason, and J. C. Wyant. J. Fleming of the Optical Society of America and V. Gagne of NIST oversaw the transcription of the manuscript from a lecture at the Optical Fabrication and Testing Workshop.

Disclaimer

Certain types of commercial equipment are mentioned in this article in order to represent adequately the type of equipment and techniques used in the field being discussed. This does not imply any endorsement of the specified equipment by the National Institute for Standards and Technology or recommendation that the equipment is the best available for the task.

References

1. American National Standard, ANSI/ASME B-46.1-1985, *Surface Texture* (American Society of Mechanical Engineers, New York, 1985).
2. T. V. Vorburger and J. Raja, *Surface Finish Metrology Tutorial, NISTIR 89-4088* (National Institute of Standards and Technology, Gaithersburg, MD, 1990).
3. J. M. Bennett and L. Mattson, *Introduction to Surface Roughness and Scattering* (Optical Society of America, Washington, DC, 1989).
4. T. R. Thomas, ed., *Rough Surfaces* (Longman, New York, 1982).
5. H. Lackenby, "Resistance of ships, with special reference to skin friction and hull surface condition," Proc. Inst. Mech. Eng. **176**, 981 (1962).
6. L. W. McKinney, "Overview of National Transonic Facility Model Technology Program," in *Cryogenic Wind Tunnel Models*, NASA Conference Publication 2262 (Natonal Aeronautics and Space Administration Langley, Hampton, VA, 1983).
7. M. Henzler and P. Marienhoff, "High resolution measurement of the step distribution at the Si/SiO_2 interface," J. Vac. Sci. Technol. **B2**, 346 (1984).
8. T. R. Thomas, ed., *Rough Surfaces* (Longman, New York, 1982), p. 18
9. T. V. Vorburger, E. C. Teague, F. E. Scire, and F. W. Rosberry, "Measurements of stylus radii," Wear **57**, 39 (1979).
10. J. F. Song and T. V. Vorburger, "Stylus profiling at high resolution and low force," Appl. Opt. **30**, 42 (1991).
11. T. V. Vorburger, F. E. Scire, and E. C. Teague, "Hydrodynamic drag versus roughness for rotating disks," Wear **83**, 339 (1982).
12. R. C. Spragg and D. J. Whitehouse, "An average wavelength parameter for surface metrology," Rev. M. Mec. **20**, 293 (1974).
13. D. G. Chetwynd, "Slope measurement in surface texture analysis," J. Mech. Eng. Sci. **20**, 115 (1978).
14. E. C. Teague, *Evaluation, Revision, and Application of the NBS Stylus/Computer System for the Measurement of Surface Roughness*, National Bureau of Standards Technical Note 902 (U.S. Department of Commerce, Washington, DC, 1976).
15. E. C. Teague, F. E. Scire, and T. V. Vorburger, "Sinusoidal profile precision roughness specimens," Wear **83**, 61 (1982).
16. R. Brodmann and W. Smilga, "Evaluation of a commercial microtopography sensor," Proc. Soc. Photo-Opt. Instrum. Eng. **802**, 165 (1987).
17. S. Tolansky, *Multiple-Beam Interference Microscopy of Metals* (Academic Press, London, 1970).
18. J. C. Wyant, C. L. Koliopoulos, B. Bhushan, and O. E. George, "An optical profilometer for surface characterization of magnetic media," ASLE Trans. **27**, 101 (1984).
19. B. Bhushan, J. C. Wyant, and C. L. Koliopoulous, "Measurement of surface topography of magnetic tapes by Mirau interferometry," Appl. Opt. **24**, 1489 (1985).
20. J. F. Biegen and R. A. Smythe, "High resolution phase-measuring interferometric microscope for engineering surface metrology," in *Metrology and Properties of Engineering Surfaces, 1988*, K. J. Stout and T. V. Vorburger, eds. (Kogan Page, London, 1988), p. 287.
21. J. M. Bennett, T. C. Bristow, K. Arackellian, and J. C. Wyant, "Surface profiling with optical and mechanical instruments," presented at the Workshop on Optical Fabrication and Testing, October 21–23, 1986, Seattle, WA, paper IV-ThB4 (Optical Society of America, Washington, DC, 1986).
22. M. J. Downs, W. H. McGivern, and H. J. Ferguson, "Optical system for measuring the profiles of supersmooth surfaces," Precision Eng. **7**, 211 (1985).

23. G. E. Sommargren, "Optical heterodyne profilometry," Applied *Optics* **20**, 610 (1981).
24. R. A. Smythe, "Heterodyne profiler moves from R & D to the marketplace," Laser Focus/Electro-Optics, 92 (July 1987).
25. R. A. Smythe, personal communication.
26. J. M. Eastman and J. M. Zavislan, "A new optical surface microprofiling instrument," Proc. Soc. Photo-Opt. Instrum. Eng. **429**, 56 (1983).
27. T. C. Bristow, "Surface roughness measurements over long scan lengths," in *Metrology and Properties of Engineering Surfaces, 1988*, K. J. Stout and T. V. Vorburger, eds. (Kogan Page, London, 1988), p. 281.
28. E. L. Church, T. V. Vorburger, and J. C. Wyant, "Direct comparison of mechanical and optical measurements of the finish of precision machined optical surfaces," Opt. Eng. **24**, 388 (1985).
29. K. Creath and J. C. Wyant, "Interferometric measurement of the roughness of machined parts," Proc. Soc. Photo-Opt. Instrum. Eng. **954**, 246 (1988).
30. G. Binnig and H. Rohrer, "Scanning tunneling microscopy," Helv. Physica Acta **55**, 726 (1982).
31. R. Young, J. Ward, and F. Scire, "The topografiner: an instrument for measuring surface microtopography," Rev. Sci. Instrum. **43**, 999 (1972).
32. G. Binnig, H. Rohrer, Ch. Gerber, and E. Weibel, "Reconstruction on Si(111) resolved in real space," Phys. Rev. Lett. **50**, 120 (1983).
33. R. A. Dragoset, R. D. Young, H. P. Layer, S. R. Mielczarek, E. C. Teague, and R. J. Celotta, "Scanning tunneling microscopy applied to optical surfaces," Opt. Lett. **11**, 560 (1986).
34. R. A. Dragoset, and T. V. Vorburger, "Scanning tunneling microscopy (STM) of a diamond-turned surface and a grating replica," Proc. Soc. Photo-Opt. Instrum. Eng. **749**, 54 (1987).
35. C. C. Williams, W. P. Hough, and S. A. Rishton, "Scanning capacitance microscopy on a 25 nm scale," Appl. Phys. Lett. **55**, 203 (1989).
36. C. C. Williams and H. K. Wickramasinghe, "Thermal and photothermal imaging on a sub-100 nanometer scale," Proc. Soc. Photo-Opt. Instrum. Eng. **897**, 129 (1988).
37. R. C. Reddick, R. J. Warmack, and T. L. Ferrell, "New form of scanning optical microscopy," Phys. Rev. B **39**, 767 (1989).
38. G. Binnig, C. F. Quate, and Ch. Gerber, "The atomic force microscope," Phys. Rev. Lett. **56**, 930 (1986).
39. S. Alexander, L. Hellemans, O. Marti, J. Schneir, V. Elings, P. K. Hansma, "An atomic-resolution atomic-force microscope implemented using an optical lever," J. Appl. Phys. **65**, 164 (1989).
40. V.B. Elings *et al.*, personal communication.
41. J. M. Bennett, J. M. Elson, P. C. Archibald, C. L. Schaub, H. L. Garvin, V. Elings, and K. Kjoller, "Comparison of scanning tunneling microscope profiles and Talystep mechanical profiler measurements of gratings and low-scatter surfaces," in OSA Annual Meeting Technical Digest, 1990 Vol. 15 of the OSA Technical Digest Series (Optical Society of America, Washington, DC, 1990), pp. 249–250.
42. D. K. Biegelsen, F. A. Ponce, J. C. Tramontara, and S. M. Koch, "Ion milled tips for scanning tunneling microscopy," Appl. Phys. Lett. **50**, 696 (1987).
43. E. L. Church, "The measurement of surface texture and topography by differential light scattering," Wear **57**, 93 (1979).
44. M. Stedman, "Basis for comparing the performance of surface-measuring machines," Precision Eng. **3**, 149 (1987).
45. J. Fu, R. D. Young, and T. V. Vorburger, to be published.
46. J. N. Brecker, R. E. Fromson, and L. Y. Shum, "A capacitance-based surface texture measuring system," CIRP Annals **25**, 375 (1977).
47. A. G. Lieberman, T. V. Vorburger, C. H. W. Giauque, D. G. Risko, and K. R. Rathbun, "Comparison of capacitance and stylus measurements of surface roughness," in *Metrology and Properties of Engineering Surfaces, 1988*, K. J. Stout and T. V. Vorburger, eds. (Kogan Page, London, 1988), p. 115.
48. T. V. Vorburger, E. C. Teague, F. E. Scire, M. J. McLay, and D. E. Gilsinn, "Surface roughness studies with DALLAS—detector array for laser light angular scattering," J. Res. Nat. Bur. Stand. **89**, 3 (1984).
49. T. V. Vorburger, L. X. Cao, C. H. W. Giauque, J. Raja, D. E. Gilsinn, and L. Fullana, "Optical scattering from rough surfaces: experiment and theory," in *Seventh International Colloquium on Surfaces*, H. Trumpold, ed. (Technische Universitat, Karl-Marx Stadt, German Dem. Rep., 1988), p. 308.
50. E. Marx, and T. V. Vorburger, "Direct and inverse problems for light scattered by rough surfaces," Appl. Opt. **29**, 3613 (1990).
51. J. H. Rakels, "Recognised surface finish parameters obtained from diffraction patterns of rough surfaces," Proc. Soc. Photo-Opt. Instrum. Eng. **1009**, 119 (1988).
52. R. Brodmann, and M. Allgauer, "Comparison of light scattering from rough surfaces with optical and mechanical profilometry," Proc. Soc. Photo-Opt. Instrum. Eng. **1009**, 111 (1988).
53. ASTM Standard F1048, *Test Method for Measuring the Effective Surface Roughness of Optical Components by Total Integrated Scattering* (ASTM, Philadelphia, 1987).
54. J. A. Detrio and S. M. Miner, "Standardized total integrated scatter measurements of optical surfaces," Opt. Eng. **24**, 419 (1985).